Solid State Ionics 232 (2013) 123–128

Contents lists available at SciVerse ScienceDirect

Solid State Ionics

journal homepage: www.elsevier.com/locate/ssi

Molecular dynamics analysis of lattice site dependent oxygen ion diffusion in $YBa_2Cu_3O_{7-\delta}$: Exposing the origin of anisotropic oxygen diffusivity

Chong Liu, Jun Zhang, Lianhong Wang, Yonghua Shu, Jing Fan *

State Key Laboratory of High-temperature Gas Dynamics, Institute of Mechanics, Chinese Academy of Sciences, Beijing 100190, China

ARTICLE INFO

Article history:
Received 3 October 2012
Received in revised form 26 November 2012
Accepted 28 November 2012
Available online 28 December 2012

Keywords:
Molecular dynamics
Oxygen
Temperature
Diffusion
Anisotropic

ABSTRACT

The oxygen diffusion in $YBa_2Cu_3O_{7-\delta}$ (YBCO) at different temperatures and oxygen contents is explored by molecular dynamics simulations. At low temperatures, the diffusivity of oxygen ions in YBCO is found to be strongly dependent on the lattice site. It is shown that the oxygen ions in Cu–O chains diffuse much faster than that in Ba–O layers and Cu–O planes. However, when temperature is increased, the diffusivity becomes less sensitive to lattice site. Moreover, distinct anisotropy is also observed for the oxygen diffusion on different lattice sites. By explicitly calculating directional mean square displacement, we show that the oxygen ions in the Cu–O planes and Ba–O layers are similarly more prone to diffuse along the *c* axis direction while in the Cu–O chains the oxygen ions are more likely to migrate along the *ab* plane. As temperature increases from 700 to 1100 K, the diffusion anisotropies decrease. The underlying microscopic origins for the above peculiarities of oxygen diffusion are analyzed.

1. Introduction

Oxygen diffusion in solids is often the limiting process controlling the rate of chemical reaction, catalysis, phase transition and oxide growth, and it has long been a central problem in solid state physics and material science [1,2]. Attention has therefore focused on the diffusivity of oxygen in solid state oxides [3–11]. Some high temperature superconductors, such as yttrium–barium cuprate ($YBa_2Cu_3O_{7-\delta}$ or YBCO), with quite promising superconductive and magnetic properties [12,13], are one case where both the oxide crystal growth and phase transitions are highly sensitive to oxygen diffusion. The atomic structures of YBCO crystal, and therefore its superconducting properties arising from particular atomic structures, depend crucially on the oxygen stoichiometry, e.g., with the decrease of δ, the phase transition from tetragonal to orthogonal takes place as well as the critical superconducting transition temperature T_c increases [14]. Ideally, to sustain the superconducting state which makes YBCO extremely appealing for a wide range of applications [15,16], fully oxygenated YBCO crystals are desired. Practically, to achieve this, a deeper physical understanding of the mechanisms of oxygen diffusion is necessitated.

Many efforts have been devoted to the investigation of oxygen diffusion in YBCO experimentally [17–19], however, in most of these studies a total bulk diffusion is assumed, the resultant kinetics of oxygen diffusion is scattered. Actually, the oxygen diffusion in solid oxides, with diverse physical situations, may take place in hierarchical orders: diffusion along surface, diffusion along grain boundary and lattice diffusion [1,2]. It is well recognized that the speed of lattice diffusion is typically much slower than that of the so called "short-circuit diffusion" including surface diffusion and grain boundary diffusion owning to different activation barriers [1,2], and thus the lattice diffusion is usually the bottleneck of oxygen transport in solid oxides. With this consideration, the kinetics of lattice diffusion is not only a clue for an overall understanding of oxygen transport in solid oxides, but this also provides a key to unveil more fundamental physics inside crystal lattice. Compared to experiments, molecular dynamics (MD) simulations offer an easy way to detect the detailed knowledge of crystal lattice [20–23]. Hence, extensive MD studies on the lattice diffusion of oxygen in various oxides with different atomic structures, e.g., the perovskite structure and double perovskite structure, have been carried out in recent years [24–28]. Nevertheless, these work rarely considered the lattice diffusion of oxygen in YBCO. Moreover, the oxygen density plots for some oxides in the recent MD analysis show that the oxygen diffusion may have distinct preferential directions on different lattice sites [3–5], which also reveal that the lattice diffusion of oxygen ions is far more complex than has been recognized so far. Although the oxygen diffusion in YBCO has been studied numerically [29], the peculiarities of oxygen diffusivity at each different lattice site in YBCO are lacking and need to be well studied.

In this study, molecular dynamics simulations are conducted to investigate the lattice diffusion of oxygen ions in YBCO. Specifically, we treat the oxygen ions at different lattice sites in YBCO as non-identical transported species according to the coordination number and chemical bond strength. With this regard, the kinetic behaviors, diffusivity and the diffusion mechanisms of different species of oxygen in YBCO under a wide range of temperature are explored. It is shown that the

* Corresponding author.
E-mail address: jfan@imech.ac.cn (J. Fan).

0167-2738/$ – see front matter © 2012 Elsevier B.V. All rights reserved.
http://dx.doi.org/10.1016/j.ssi.2012.11.022

mobility of oxygen is strongly dependent on the lattice site for low temperatures. However, as the temperature increases, the oxygen diffusion becomes less lattice site dependent. Moreover, distinct anisotropic oxygen diffusion is also captured by MD simulations at different lattice sites, and the mechanisms underlying these diffusion anisotropies are disclosed.

2. Molecular dynamics simulation

The MD simulation is performed under constant temperature, pressure and number of atoms (NPT ensemble) for YBCO using the Large-scale Atomic/Molecular Massively Parallel Simulator (LAMMPS) [30,31] developed at the Sandia National Laboratories. The orthorhombic unit cell of the superconducting $YBa_2Cu_3O_7$ is shown in Fig. 1(a), the stacking layers of YBCO along the *c* axis are CuO_2/Y/CuO_2/BaO/CuO/BaO, where Y layer is sandwiched by two Cu–O planes, and Cu–O chain is located between two Ba–O layers. In YBCO, Cu–O plane contains three lattice sites [Cu(2),O(2) and O(3)], Ba–O layer has two sites [Ba and O(4)], and Cu–O chain includes Cu(1) and O(1), as depicted in Fig. 1(a). The initial configuration of the simulation model is illustrated in Fig. 1(b), which contains $10\times10\times4$ unit cell of YBCO. The orthogonal coordinates of the *a*, *b*, and *c* axes are set, respectively, along the [100], [010] and [001] lattice directions for all the simulations. Periodic boundary conditions are applied in all directions. Initially, random velocities that follow the Maxwell–Boltzmann distribution corresponding to the desired temperature are assigned to the ions. The Nose–Hoover thermostat and barostat are employed to control temperature and stress of simulation system at the desired values respectively.

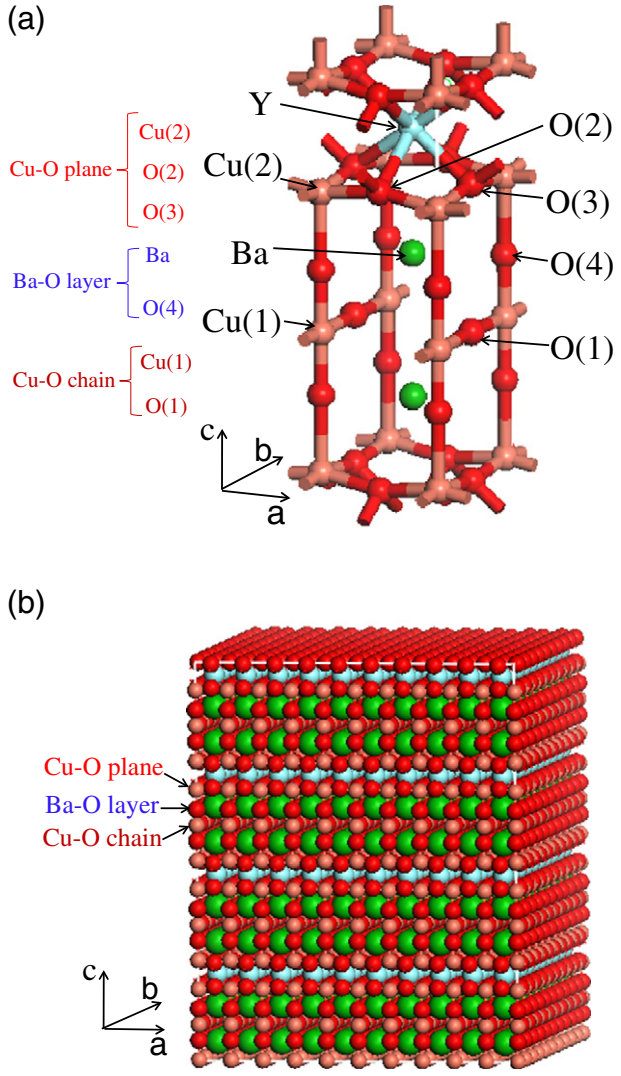

Fig. 1. (a) Structure and model unit of layered $YBa_2Cu_3O_7$, and, (b) the initial configuration of $YBa_2Cu_3O_7$ in the molecular dynamics simulation. When the oxygen content is <7, O(1) sites are partially filled.

In this work, we employ an empirical pairwise potential, which gives good predictions on the structure and dynamics of YBCO [29], and its general form is as follow:

$$U_{kk'}\left(r_{ij}\right)=\frac{e^2Z(k)Z\left(k'\right)}{4\pi\varepsilon_0 r_{ij}}+a\ \exp\left[\frac{-br_{ij}}{R(k)+R\left(k'\right)}\right]-\frac{w}{r_{ij}^{\ 6}}-cD\ \exp\left[\frac{-n\left(r_{ij}-r_0\right)^2}{2cr_{ij}}\right] \quad (1)$$

where r_{ij} is distance between ions of species *k* and *k*′, $Z(k)$ and $Z(k')$ are the effective charges, $e^2/(4\pi\varepsilon_0)=144$ eV/nm, $a=1822$ eV and $b=12.364$ [29]. It is stressed that the first two terms of the right side of Eq. (1) are applied to calculate interactions between all species of ions. However, the third term is assumed to act only between any two oxygen ions. The fourth term, a covalent potential of the Lippincott–Schroeder type, is only assumed between copper and oxygen ions that are either in the Cu–O planes or in Cu–O chains [29]. The parameters in the third and fourth terms are chosen as $w=50\times10^{-6}$ eV nm^6, $c=0.5$, $D=1$ eV, $n=80$ nm^{-1}, and $r_0=0.18$ nm [29,32], which are good for considering the high-temperature behavior of YBCO [32]. The values of $Z(k)$ and $R(k)$ for the cases of $\delta=0$ and 1 are listed in Table 1, from which the values for other cases ($0<\delta<1$) can be interpolated [29]. As δ increases, oxygen may diffuse out of the crystal, and then the oxygen vacancies occur at O(1) site. Therefore, in the initial configuration of the MD models, O(1) site may be partially filled according to the variation of δ. As required by the charge neutrality, positive charge is depleted from Cu (1) and Ba with decreasing oxygen stoichiometry (increasing δ), as shown in Table 1 [29]. In this simulation, the long range coulombic interactions are handled by Ewald summation [33], and the short range interactions are truncated at 10 Å. With the time step equals 1 fs, the system is relaxed for 100 ps before the mean square displacement and other properties of the ions are measured.

To quantify the ionic transport, we record the mean square displacement (MSD) as a function of simulation time through tracking the trajectory of each ion in the system. In the present MD simulations, the MSD is determined by,

$$\left\langle r_i^{\ 2}(t)\right\rangle=\frac{1}{N}\sum_{i=1}^{N}\left[r_i(t)-r_i(0)\right]^2 \quad (2)$$

where *N* is the total number of ions in the system, $r_i(t)$ is the position of ion *i* at time *t* and $r_i(0)$ is the initial position of ion *i*. The diffusion coefficients of the ionic species, *D*, are obtained directly from the MSD of the ions according to the Einstein relation,

$$\left\langle r_i^{\ 2}(t)\right\rangle=B+6D\Delta t \quad (3)$$

Table 1
Interionic potential parameters for $YBa_2Cu_3O_{7-\delta}$ [see Eq. (1)]. From ref. [29].

	δ=0		δ=1	
Atom	Z	R (nm)	Z	R (nm)
Y	1.9	0.178	1.9	0.178
Ba	1.5	0.230	1.25	0.210
Cu(1)	1.4	0.120	0.6	0.110
Cu(2)	1.4	0.120	1.4	0.120
O	−1.3	0.174	−1.3	0.174

where B is a constant and Δt is the time interval to obtain the mean square displacement. To reduce statistical noise, a sufficient long MD run, 500 ps, is performed to monitor the trajectories of oxygen ions for all the simulations.

3. Results and discussion

We first compute the evolution of the mean square displacement of all the oxygen ions in YBCO crystal as a function of simulation time at different temperatures, as shown in Fig. 2(a). It can be seen that the MSD is generally proportional to simulation time, and also as temperature increases from 700 K to 1100 K the MSD raises accordingly. The diffusion coefficients of all the oxygen ions in YBCO crystal for different temperatures can be evaluated from the relationship between the MSD and time in Fig. 2(a) with Eq. (3). Arrhenius plot of the diffusion coefficient versus reciprocal temperature is illustrated in Fig. 2(b), where the symbols are the simulation data points and solid lines are the linear fit to the data. Briefly, within the temperature range considered in this work, the diffusivity of the whole oxygen ions in YBCO crystal follows the Arrhenius law and increases with increasing temperature. Additionally, our data in Fig. 2(b) also indicates that the oxygen diffusivity in high oxygen content $YBa_2Cu_3O_{7-\delta}$ crystal ($\delta = 0$) stays somewhat above the diffusivity in low oxygen content $YBa_2Cu_3O_{7-\delta}$ crystal ($\delta = 0.4$). This difference could be attributed mostly to the decreasing occupancy of O(1) sites by oxygen ions with increasing δ on condition that the diffusion ability of each oxygen ion depends on the lattice site it belongs to.

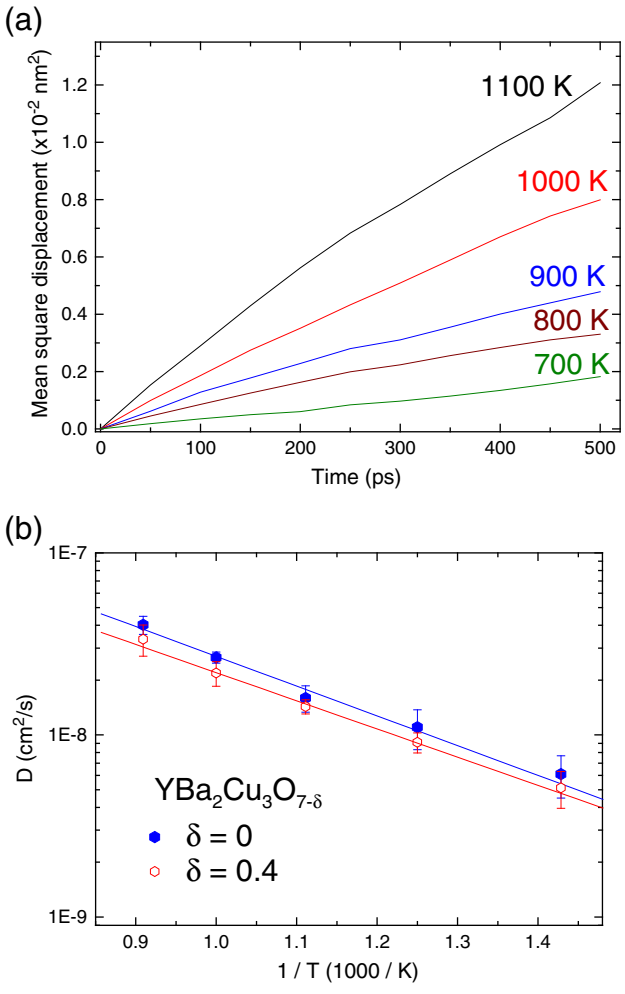

Fig. 2. (a) Mean square displacement of oxygen ions in $YBa_2Cu_3O_7$ as a function of time at different temperatures. (b) Arrhenius plot of the diffusion coefficient of oxygen ions in $YBa_2Cu_3O_{7-\delta}$ as a function of reciprocal temperature. Linear fit to the data is also shown. The error bars are caused by the divergence of simulation results from different initial conditions.

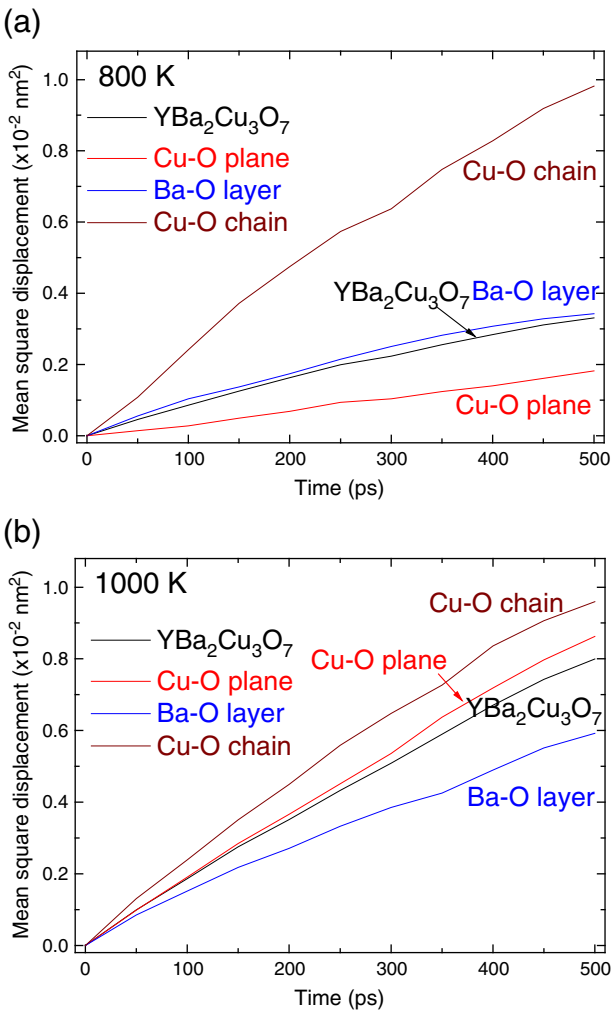

Fig. 3. Mean square displacement of oxygen ions at different lattice sites in $YBa_2Cu_3O_7$. (a) 800 K and (b) 1000 K.

In the following, we therefore treat the oxygen ions on different lattice sites as different species of ions with regard to the variation of coordination number and chemical bond strength. As illustrated

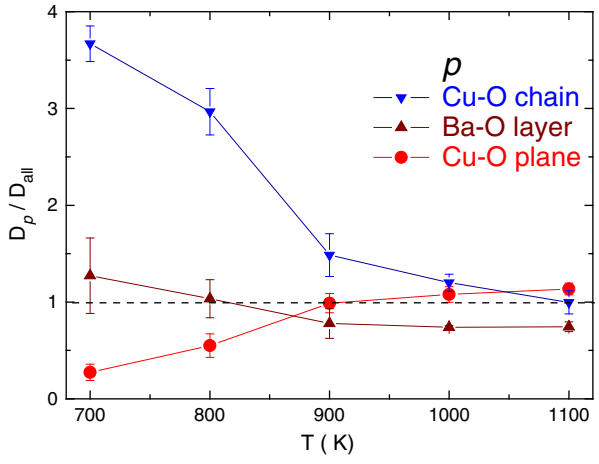

Fig. 4. The ratio of diffusion coefficient of the oxygen ions at different lattice sites to the diffusion coefficient of all the oxygen ions in $YBa_2Cu_3O_7$ as a function of temperature.

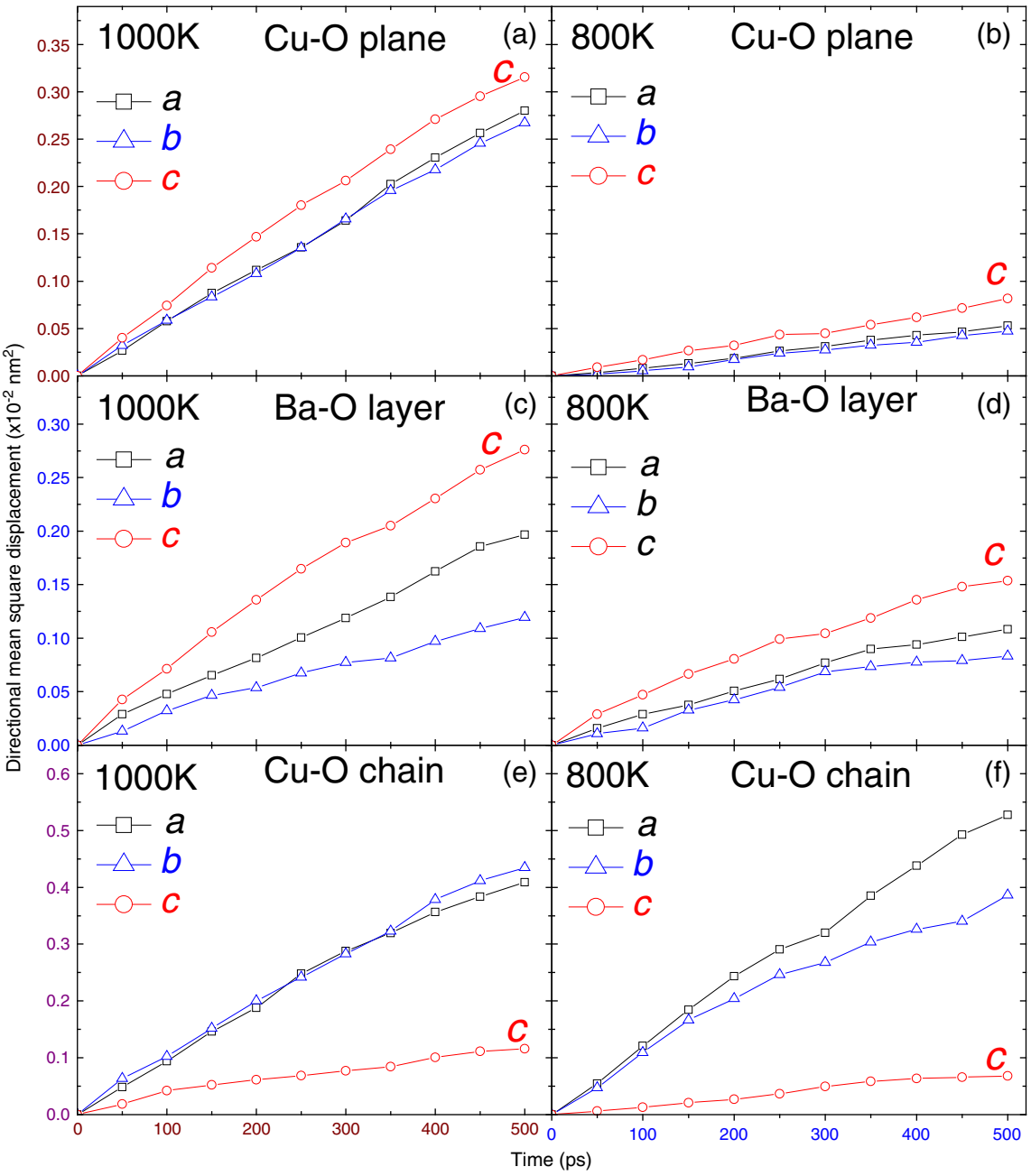

Fig. 5. Mean square displacement of oxygen ions at different lattice sites along the three orthogonal directions. (a) and (b) are for the oxygen ions in Cu–O planes at 1000 K and 800 K, (c) and (d) are for the oxygen ions in Ba–O layers at 1000 K and 800 K, (e) and (f) are for the oxygen ions in Cu–O chains at 1000 K and 800 K.

by the atomic structure in Fig. 1(a), the oxygen ions in YBCO are divided into three groups, which include the oxygen ions in the Cu–O planes, Ba–O layers and Cu–O chains. In different groups, the oxygen ions are connected with different species of cation, e.g., the oxygen ions in the Cu–O planes are bonded with Cu(2) and Y ions, while the oxygen ions in the Cu–O chains are connected with the Cu(1). Therefore, the local oxygen-cation bond strength is strongly dependent on lattice site. Within each group, oxygen ions have similar local situations, i.e., species of their neighboring cations, strength of the interionic interaction and even directions of chemical bond are no big difference. Hence, it is reasonable to view the oxygen ions in each group as the identical species. For the purpose of detecting the dependence of the oxygen diffusivity on the lattice position, the MSD of oxygen ions in each group is calculated individually. It is evident from Fig. 3(a) that the diffusivity and mobility of oxygen ions in YBCO strongly depends on lattice site, e.g., the oxygen ions in Cu–O chains have the largest mobility due to several reasons, including weak chemical bond and large number of neighboring oxygen vacancies, all of which may enhance the local diffusivity greatly. This interprets why the diffusion coefficient of all the oxygen ions in YBCO changes with δ, as discussed in the previous paragraph.

Comparison of Fig. 3(a) and (b) suggests that high temperature would evidently reduce the dispersion of MSD of the oxygen ions at different lattice sites. This trend gives the impression that there should exit a transition from lattice site dependent diffusion regime to lattice site insensitive diffusion regime with increasing temperature. To verify this, we calculate the diffusion coefficient of oxygen ions at different lattice positions D_p under a wide range of temperature (the subscript p could be Cu–O plane, Ba–O layer, and Cu–O chain, which indicates the lattice position where the oxygen ions initially rest on). The transition of oxygen diffusion from strong to weak site-dependent is better illustrated by the ratio of D_p/D_{all} as a function of temperature (Fig. 4),

where D_{all} is the diffusion coefficient of all the oxygen ions in YBCO crystal. It is seen that when the temperature is below 900 K, the ratio of D_p/D_{all} may deviate significantly from unity, which confirms that at low temperature the oxygen diffusion lies in the site-dependent diffusion regime. With the increase of temperature, the ratio of D_p/D_{all} for different lattice sites tend to converge, the oxygen diffusion therefore becomes less sensitive to lattice site.

The strong dependence of the oxygen diffusivity on lattice site at low temperature may arise from the variation of ionic bond strength. This explanation, however, belies a large complexity which requires more detailed investigation. Inspired by the recent MD studies of the anisotropic oxygen diffusion in other perovskite compounds [3–5], we examine the projection of oxygen MSD in YBCO along the three orthogonal directions, i.e., the directions along the *a*, *b*, and *c*-axes. The directional MSD of oxygen ions at different lattice sites is plotted as a function of time in Fig. 5. It is shown that the oxygen ions in Cu–O planes and Ba–O layers similarly have the largest directional MSD along the *c*-axis direction [Fig. 5(a)–(d)], which indicates that the oxygen ions in these locations are more prone to diffuse along the *c*-axis direction. However, for the oxygen ions in the Cu–O chains, the directional MSD along the *a* and *b*-axis directions is significantly larger than that along the *c*-axis direction, as shown by Fig. 5(e) and (f). This implies that the oxygen ions on Cu–O chains are easy to diffuse along the *ab* plane rather than along the *c*-axis direction. It is also noted that the oxygen diffusion in Cu–O planes is more sensitive to temperature than that in the Ba–O layers [Fig. 5(a)–(d)]. For example, as temperature decreases from 1000 K to 800 K, the MSD of oxygen ions in Cu–O planes is reduced by a factor of 5, which is larger than that in Ba–O layers. This help us to understand why the diffusivity of oxygen ions in the Ba–O layers is larger than that in the Cu–O planes at low temperature, while with the increasing of temperature the situation changes, as shown in Fig. 4. Moreover, Fig. 5(e) and (f) also reveals that the oxygen diffusion in the Cu–O chains is almost independent of temperature within the range from 1000 K to 800 K, especially for the diffusion along the *a* or *b* axis direction due to small diffusion barriers.

To demonstrate the atomistic mechanisms of the anisotropic oxygen diffusion as implicated by the dispersion of the directional MSD in Fig. 5, we examine the trajectories of oxygen ions obtained at 800 K. The snapshot in Fig. 6(a) shows the initial configuration of the whole oxygen ions in YBCO, and Fig. 6(b), (c) and (d) shows the finial configurations of oxygen ions initially in Cu–O planes, Ba–O layers and Cu–O chains respectively. Comparison of the red particles in Fig. 6(b) with their initial configuration in Fig. 6(a) illustrates that most of the oxygen ions in the Cu–O plane are thermally vibrating around their equilibrium positions, only a few of them can occasionally diffuse out of the plane and hop into their neighboring Ba–O layers. In addition, the snapshots in Fig. 6(c) and (d) show that almost no oxygen ions from the Ba–O layers or Cu–O chains can penetrate into or through the Cu–O plane during the whole simulation time. This would mean that the highly dense Cu–O plane can be viewed as a fence to suppress the long distance oxygen diffusion along the *c* axis direction in YBCO especially for low temperature. Similar to the case in Cu–O planes, the oxygen ions in Ba–O layers are also not easy to diffuse along the *a* or *b* axis direction due to large diffusion barrier, however, they are more prone to jump out of Ba–O layers firstly, and then diffuse along the *a* or *b* axis within the high oxygen vacancy regions where the Cu–O chains are located [Fig. 6(c)]. On the contrary, the oxygen ions in Cu–O chains can easily move fast along the *a* or *b* axis direction within the regions between each two neighboring Ba–O layers, some of them may also migrate into the Ba–O layers to occupy oxygen vacancies, as illustrated by Fig. 6(c). In this case, the regions between each two neighboring Ba–O layers act as effective channels to transport oxygen ions.

The anisotropy of the oxygen diffusivity may strongly depend on temperature. To quantify this, we calculate the directional diffusion coefficient based on directional MSD in Fig. 5. As previously discussed, the oxygen ions in layered YBCO have two distinct preferential diffusion directions, i.e., one is along the *ab* plane and the other is along the *c* axis direction, therefore the ratio of $D_{a(b)}/D_c$ can be used to describe the diffusion anisotropies, where $D_{a(b)}$ represents directional diffusion coefficient along the *a* or *b* axis direction, as shown in Fig. 7. For low temperatures, the ratio of $D_{a(b)}/D_c$ for oxygen ions on Cu–O chains is evidently larger than 1, which is comparable to the value of $D_{a(b)}/D_c$ for the oxygen diffusion in $GdBaCo_2O_{5.5}$ due to similar layer-by-layer perovskite structure [5]. As temperature increases, $D_{a(b)}/D_c$ decreases significantly and approaches to unity (Fig. 7). For the oxygen ions in Cu–O planes and Ba–O layers, $D_{a(b)}/D_c$ is typically smaller than 1, which confirms that the oxygen favors to migrate along the *c* axis direction. Similarly, with increasing temperature, it also gets close to unity. The change of $D_{a(b)}/D_c$ with temperature in Fig. 7 implies that the anisotropy decreases with increasing temperature. These temperature sensitive anisotropies could be ascribed to the direction-dependent diffusion barrier. When the temperature is low, oxygen ions may not have enough kinetic energy to overcome large potential barrier and then they are more likely to migrate along the direction with small diffusion barrier, as a result the diffusion anisotropy is obvious. However, at high temperatures, large kinetic energy enables the oxygen ions to diffuse more freely, and consequently the diffusion anisotropy decreases.

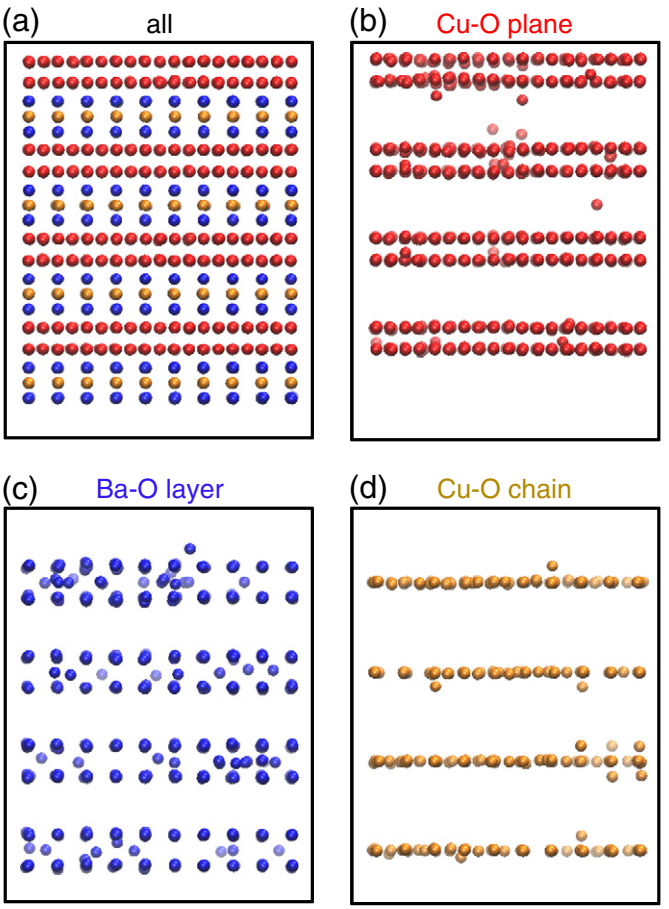

Fig. 6. The snapshots of the oxygen ions in YBCO lattice crystal. (a) The front view of the initial configuration of all oxygen ions, (b), (c) and (d) are the finial configurations of oxygen ions in Cu–O planes, Ba–O layers and Cu–O chains, as denoted by the red, blue and yellow spheres respectively.

4. Conclusion

In summary, we report a series of molecular dynamics calculations on the lattice diffusion of oxygen ions in YBCO. When the temperature is lower than 900 K, it is found that oxygen diffusivity strongly

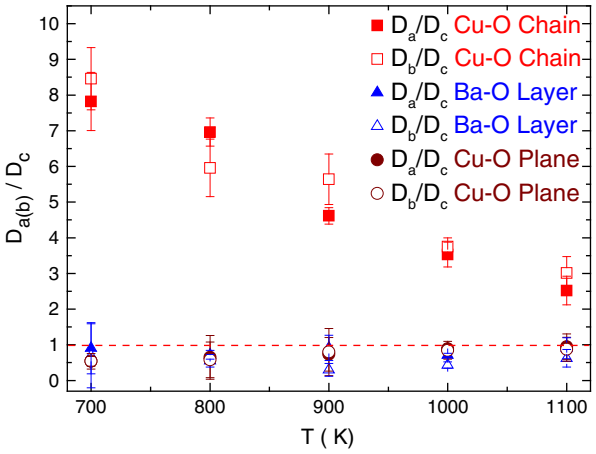

Fig. 7. The ratio of oxygen diffusion coefficient in the *a* or *b*-axis direction to that in the *c*-axis direction versus temperature.

depends on the lattice site, and the diffusion coefficient of oxygen ions in the Cu–O chains is much larger than that in Ba–O layers and Cu–O planes. However, as the temperature increases, the oxygen diffusion becomes less site-dependent. In addition, distinct anisotropic oxygen diffusion is observed at different lattice sites, the oxygen ions in Cu–O planes and Ba–O layers are more prone to diffuse along the *c* axis, however, the oxygen ions on Cu–O chains are much easier to migrate in the *ab* plane. We also show that the diffusion anisotropy decreases with increasing temperature. The insight into the above fundamental issues can also be used to particularize our understanding of oxygen diffusion in some more complicated lattice structures.

Acknowledgments

This work was supported by the National Natural Science Foundation of China (grant nos. 10921062 and 11002147).

References

[1] P.H.J. Kärger, Diffusion in Condensed Matter Methods, Materials, Models, Springer, Berlin Heidelberg, 2005.
[2] H. Schmalzried, Chemical Kinetics of Solids, VCH, Weinheim, 1995.
[3] D. Rupasov, A. Chroneos, D. Parfitt, J.A. Kilner, R.W. Grimes, S.Y. Istomin, E.V. Antipov, Phys. Rev. B 79 (2009) 172102.
[4] I.D. Seymour, A. Tarancon, A. Chroneos, D. Parfitt, J.A. Kilner, R.W. Grimes, Solid State Ionics 216 (2012) 41–43.
[5] J. Hermet, G. Geneste, G. Dezanneau, Appl. Phys. Lett. 97 (2010) 174102.
[6] J. Hermet, B. Dupe, G. Dezanneau, Solid State Ionics 216 (2012) 50–53.
[7] C.A.J. Fisher, M. Yoshiya, Y. Iwamoto, J. Ishii, M. Asanuma, K. Yabuta, Solid State Ionics 177 (2007) 3425–3431.
[8] M. Machida, T. Shiomitsu, K. Eguchi, H. Haneda, H. Arai, J. Mater. Chem. 2 (1992) 455–458.
[9] H.I. Yoo, B.J. Wuensch, W.T. Petuskey, Solid State Ionics 150 (2002) 207–221.
[10] H. Kanai, T. Hashimoto, H. Tagawa, J. Mizusaki, Solid State Ionics 99 (1997) 193–199.
[11] L. Wang, R. Merkle, J. Maier, T. Acartürk, U. Starke, Appl. Phys. Lett. 94 (2009) 071908.
[12] J.L. Macmanus-Driscoll, S.R. Foltyn, Q.X. Jia, H. Wang, A. Serquis, L. Civale, B. Maiorov, M.E. Hawley, M.P. Maley, D.E. Peterson, Nat. Mater. 3 (2004) 439–443.
[13] D.P. Norton, A. Goyal, J.D. Budai, D.K. Christen, D.M. Kroeger, E.D. Specht, Q. He, B. Saffian, M. Paranthaman, C.E. Klabunde, D.F. Lee, B.C. Sales, F.A. List, Science 274 (1996) 755–757.
[14] J.D. Jorgensen, B.W. Veal, A.P. Paulikas, L.J. Nowicki, G.W. Crabtree, H. Claus, W.K. Kwok, Phys. Rev. B 41 (1990) 1863–1877.
[15] D. Larbalestier, A. Gurevich, D.M. Feldmann, A. Polyanskii, Nature 414 (2001) 368–377.
[16] J. Beyer, D. Drung, F. Ludwig, T. Minotani, K. Enpuku, Appl. Phys. Lett. 72 (1998) 203–205.
[17] K.N. Tu, S.I. Park, C.C. Tsuei, Appl. Phys. Lett. 51 (1987) 2158–2160.
[18] S.J. Rothman, J.L. Routbort, J.E. Baker, Phys. Rev. B 40 (1989) 8852–8860.
[19] K.N. Tu, N.C. Yeh, S.I. Park, C.C. Tsuei, Phys. Rev. B 39 (1989) 304–314.
[20] H. Hayashi, R. Sagawa, H. Inaba, K. Kawamura, Solid State Ionics 131 (2000) 281–290.
[21] H. Inaba, R. Sagawa, H. Hayashi, K. Kawamura, Solid State Ionics 122 (1999) 95–103.
[22] R.L. Gonzalez-Romero, J.J. Melendez, D. Gomez-Garcia, F.L. Cumbrera, A. Dominguez-Rodriguez, F. Wakai, Solid State Ionics 204 (2011) 1–6.
[23] T.P. Perumal, V. Sridhar, K.P.N. Murthy, K.S. Easwarakumar, S. Ramasamy, Comput. Mater. Sci. 38 (2007) 865–872.
[24] Y. Yamamura, S. Kawasaki, H. Sakai, Solid State Ionics 126 (1999) 181–189.
[25] T. Arima, K. Fukuyo, K. Idemitsu, Y. Inagaki, J. Mol. Liq. 113 (2004) 67–73.
[26] R. Devanathan, W.J. Weber, S.C. Singhal, J.D. Gale, Solid State Ionics 177 (2006) 1251–1258.
[27] W. Araki, Y. Arai, Solid State Ionics 181 (2010) 1534–1541.
[28] W. Araki, Y. Arai, Solid State Ionics 190 (2011) 75–81.
[29] S.L. Chaplot, Phys. Rev. B 42 (1990) 2149–2154.
[30] http://lammps.sandia.gov/index.html.
[31] S. Plimpton, J. Comput. Phys. 117 (1995) 1–19.
[32] S.L. Chaplot, Phase Transitions 19 (1989) 49–59.
[33] P.P. Ewald, Ann. Phys. 64 (1921) 253–287.